REVIEW OF BEAM INSTABILITIES IN THE PRESENCE OF ELECTRON CLOUDS IN THE LHC

Kevin Li, G. Rumolo, CERN, Geneva, Switzerland

Abstract

Recent observations at the LHC indicate the build-up of electron clouds when 50 ns spaced beams are injected into the machine at nominal intensity. These electron clouds are a source of coherent beam instabilities and incoherent emittance growth and limit the achievable luminosity. To better understand the influence of electron clouds on the beam dynamics, simulations have been carried out to study both the coherent and the incoherent effects on the beam. The simulations are performed with the HEADTAIL tracking code [2]; the usage of new post-processing software allows determining not only the beam intensity thresholds in terms of the central electron cloud density but also the footprint of the beam in tune space. In this paper we review instability thresholds and tune footprints for beams with different emittances and interacting with an electron cloud in field-free or dipole regions.

INTRODUCTION

In the Large Hadron Collider (LHC) the build up of electron clouds can pose a serious limitation on the peak luminosity [1]. Electron clouds can be seeded by residual gas ionisation or photoemission. Primary electrons extract energy from the circulating beam, which enables them to generate secondary electrons, thus leading to an avalanche effect. After a certain number of injected bunches, a stationary distribution of electron cloud can be established in the machine. The circulating beam interacts with this electron cloud and the interaction is determined by the particle distribution within the beam as well as within the electron cloud. Hence, it represents a collective effect.

In an effort to increase the peak luminosity in 2010 the bunch spacing in the LHC was reduced from 75 ns to 50 ns at a nominal bunch intensity of 1.15×10^{11} ppb. Indications of electron cloud build-up and resulting beam instabilities were observed. The electron cloud effects could be mitigated by means of a scrubbing run providing an in-situ surface treatment of the machine. Nevertheless, it became evident that an improved understanding of the build-up and the instability mechanism was necessary, especially in view of potential luminosity upgrades in the near future. For this reason a simulation study has been launched to estimate the threshold values for coherent instabilities induced by electron clouds in the LHC. Threshold values have been determined for straight sections and for bends at flat-bottom (450 GeV) and at the present flat-top (3.5 TeV) energy and for different transverse normalised emittances. All simulations were performed with HEADTAIL electron cloud flavour.

NUMERICAL MODEL

Simulations of collective effects usually require multi-particle tracking codes. HEADTAIL has been chosen as simulation tool for this study. It includes a number of different collective effects, is easily extensible and has been well bench-marked in the past. Recent upgrades of the code, which include a new data model and new data processing, not only allow for the study of the coherent bunch motion but also of the incoherent beam dynamics.

The tracking is based on beam transport by subsequent application of linear transport matices and kicks. For this, the ring is split into a discrete set of transport sections and interaction points. The bunch is transported along a section by means of Twiss maps according to the local (α, β, γ)-parameters. At the end of each section the bunch interacts with an electron cloud (or any other source of impedance). The electron clouds are assumed to be 2D uniform rectangular distributions of electrons. The bunch is sliced longitudinally and the interaction with the electron cloud takes place slice by slice. The computation of the bunch-electron cloud interaction itself is performed using a Particle-In-Cell FFT-type Poisson solver.

As the bunch passes through the electron cloud, the electrons are attracted towards the bunch and the cloud is pinched. Slices towards the back are affected depending on the statistical properties of the slices towards the front which causes head-tail coupling.

Thus, the bunch-electron cloud interaction can give rise to coherent bunch modes which under certain conditions may become unstable. The coherent instability can be detected as an exponential growth of the emittance from statistical noise. As the emittance increases a saturation of the instability is observed. One of the reasons for this, is the weakening of the electron cloud due to the emittance increase, which damps the rise of the coherent instability.

This type of interaction may also induce incoherent emittance growth. It can generate large tune spreads and promote interactions of single particles with the non-linearities of the machine but also with the intrinsically non-linear electron-cloud itself by periodic crossing of resonances. Incoherent instabilities are detected as a linear growth of the emittance.

Incoherent emittance growth should be interpreted with care, however. It becomes dominant when either a single interaction is highly pronounced or when the integrated force of all interactions over one turn exceeds a certain threshold. In both cases the tune spread and the resulting incoherent emittance growth become so strong that any coherent effect is suppressed. Since the distribution of the electron clouds along the ring is not known, the resonances

05 Beam Dynamics and Electromagnetic Fields

D05 Instabilities - Processes, Impedances, Countermeasures

excited in the simulation can be rather artificial. Nevertheless, the shape of the tune footprint gives an indication on what resonances might be crossed and can become a potential source of emittance degradation.

COHERENT EMITTANCE GROWTH

To study the threshold values for coherent instabilities both at 450 GeV and at 3.5 TeV, the central cloud density was scanned for different values of the bunch intensity and of the transverse emittance. The rise times of the resulting emittance curves were determined for each case assuming the emittance evolution is described as

$$\varepsilon_n(t) = \varepsilon_0 + a \, \exp\left(\frac{t}{\tau}\right) , \tag{1}$$

where ε_0 is the stationary solution and the second term in eq. (1) describes the evolution of the coherent perturbation with some amplitude a and the rise time τ. The instability threshold was set at rise times below 10 ms. The number of kick sections per turn was set to 101 and was chosen to suppress any artificial enhancement of the incoherent emittance growth.

Straight Section

Figure 1 shows a typical scan of the central cloud density at flat-bottom at nominal intensity and at a transverse normalised emittance of 2.5 μm. The emittance curves are plotted on the left graph together with the corresponding rise time values on the right graph. The dependency of the rise times versus the central cloud density for this particular case is best approximated by $\tau \sim \rho_e^{-3.48}$. At low central densities the rise times are in the order of several seconds indicating that a coherent emittance growth is likely to be damped by other mechanisms.
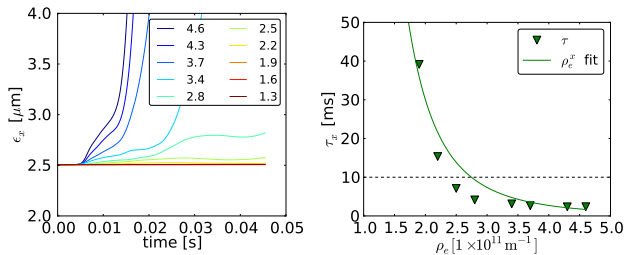
Figure 1: Left: emittance evolution for different central cloud densities at an energy of 450 GeV. The legend entries indicate the central cloud densities in $1 \times 10^{11} \, \mathrm{m}^{-3}$. Right: corresponding rise time values with threshold set at 10 ms.

Figure 2 shows the same scan at flat-top. At this energy the dependency of the rise times versus the central cloud density is approximated by $\tau \sim \rho_e^{-1.96}$. It is less steep than for the low energy case and as a result, the instability threshold is shifted towards higher values. On the
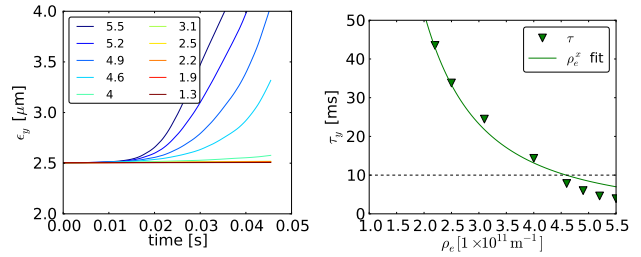
Figure 2: Left: emittance evolution for different central cloud densities at an energy of 3.5 TeV. The legend entries indicate the central cloud densities in $1 \times 10^{11} \, \mathrm{m}^{-3}$. Right: corresponding rise time values with threshold set at 10 ms.

other hand, at low central densities the rise times are comparatively small and a coherent emittance growth emerges rather early. For both cases the coherent growth is clearly visible when the rise time decreases below 10 ms.

Figure 3 summarizes the instability threshold values obtained for the straight section for both flat-bottom and flat-top energy and different transverse emittances. As expected, the threshold values decrease together with the transverse emittances as a result of the reduced beam sizes. The dependency of the threshold on the bunch intensity is weak at low energy and becomes pronounced at higher energies. Thus, at low bunch intensities the thresholds start off higher at high energy. As the bunch intensity increases, the thresholds at high energy fall below the thresholds at low energy. In all cases the thresholds appear to saturate with increasing bunch intensity.
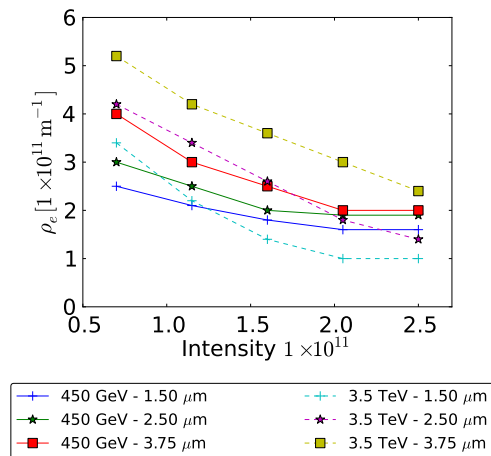
Figure 3: Instability threshold values for the straight section for 450 GeV and 3.5 TeV for different transverse emittances.

Bending Magnets

As opposed to the straight sections, in the bending magnets the electrons are forced to move along the magnetic

field lines. Thus, their motion is restricted to the vertical plane. As a result, the impact of the cloud on the beam is strongly reduced in the horizontal plane and potential instabilities occur solely in the vertical plane.

Figure 4 again shows a typical scan of the central cloud density at flat-bottom at nominal intensity and at a transverse normalised emittance of 2.5 μm. The emittance curves are plotted on the left graph together with the corresponding rise time values on the right graph. The dependency of the rise times versus the central cloud density is approximated by $\tau \sim \rho_e^{-1.46}$.
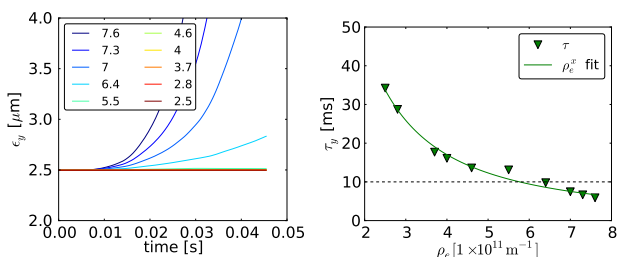
Figure 4: Left: emittance evolution for different central cloud densities at an energy of 450 GeV. The legend entries indicate the central cloud densities in 1×10^{11} m^{-3}. Right: corresponding rise time values with threshold set at 10 ms.

For the case of the bending magnets, at flat-top no coherent instabilities were observed within the scan range of the central cloud densities (up to $\rho_e = 1.03 \times 10^{12}$ m^{-3}).

Figure 5 summarizes the instability threshold values obtained for the bending magnets at injection energy. Again, the threshold values decrease together with the transverse emittances as a result of the reduced beam sizes. Compared to the straight section, however, the threshold values are roughly a factor 2 higher.
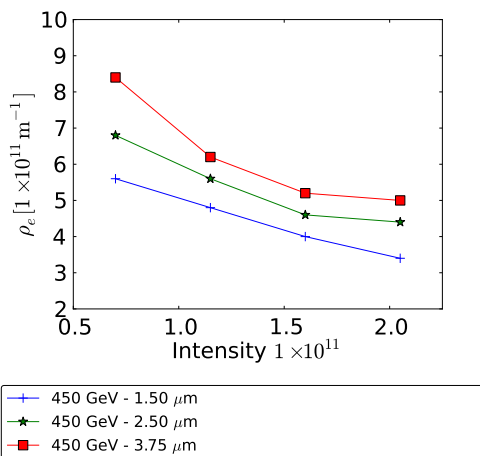
Figure 5: Instability threshold values for the bending magnets at 450 GeV for different transverse emittances.

INCOHERENT EFFECTS

Figure 6 shows the tune footprints at injection energy for the straight sections and for the bending magnets for a transverse emittance of 2.5 μm. The footprints are accumulated over 10 turns. Red dots indicate particles at the head of the bunch, blue dots are particles at the tail. In the straight sections, particles in the center region of the bunch experience the largest impact of the cloud. The same is true for the bending magnets where, however, the tune spread is dominant in the vertical plane. In addition, a folding of the footprint can be observed.
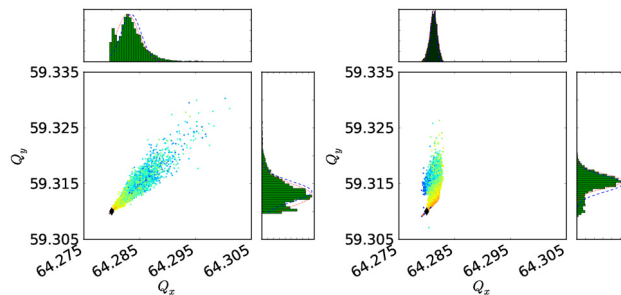
Figure 6: Left: tune footprint in the straight sections. Right: tune footprint in the bending magnets. Particles at the head are red, particles towards the tail are blue.

CONCLUSIONS

In this paper coherent instabilities induced by electron clouds in the LHC have been reviewed at both injection energy and at 3.5 TeV for the straight sections as well as for bending magnets. In all cases, the instability threshold decreases for lower values of the transverse emittance. The threshold values in the bending magnets are at least a factor 2 higher than in the straight sections. For the examined bunch intensities, typical threshold values in the straight sections are in the order of $2–4 \times 10^{11}$ m^{-3} at injection energy and $1–5 \times 10^{11}$ m^{-3} at 3.5 TeV. Threshold values in the bending magnets are in the order of $3 - 9 \times 10^{11}$ m^{-3} at injection energy.

Tune footprints were obtained below the instability threshold at injection energy. The incoherent tune spread is larger for the straight sections compared to the bending magnets. In addition, for the bending magnets the incoherent tune spread is dominant in the vertical plane. Tune spreads are in the order of 2.5×10^{-3} for the straight sections and 2.1×10^{-3} for the bending magnets.

REFERENCES

[1] G. Rumolo *et al.*, THOBA01 these proceedings.

[2] G. Rumolo and F. Zimmermann, "Practical User Guide for HEADTAIL", CERN-SL-Note-2002-036, 2002.